Nano Energy 96 (2022) 107066

Contents lists available at ScienceDirect

Nano Energy

journal homepage: www.elsevier.com/locate/nanoen

Full paper

Revealing the superlative electrochemical properties of o-B_2N_2 monolayer in Lithium/Sodium-ion batteries

Nabil Khossossi [a], Wei Luo [a,*], Zakaryae Haman [b], Deobrat Singh [a], Ismail Essaoudi [b], Abdelmajid Ainane [b], Rajeev Ahuja [a,c,*]

[a] Condensed Matter Theory Group, Materials Theory Division, Department of Physics and Astronomy, Uppsala University, Box 516, 75120 Uppsala, Sweden
[b] Laboratoire de Physique des Matèriaux et Modélisations des Systèmes, (LP2MS), Unité Associée au CNRST-URAC 08, Faculty of Sciences, Department of Physics, Moulay Ismail University, Meknes, Morocco
[c] Department of Physics, Indian Institute of Technology Ropar, Rupnagar 140001, Punjab, India

ARTICLE INFO

Keywords:
Lithium and sodium ion battery
2D orthorhombic diboron dinitride
o-B_2N_2
Electrochemical properties
First principles calculations

ABSTRACT

Promising flexible electrochemical energy storage systems (EESSs) are currently drawing considerable attention for their tremendous prospective end-use in portable self-powered electronic devices, including roll-up displays, and "smart" garments outfitted with piezoelectric patches to harvest energy from body movement. However, the lack of suitable battery electrodes that provides a specific electrochemical performance has made further development of these technologies challenging. Two-dimensional (2D) lightweight and flexible materials with outstanding physical and chemical properties, including mechanical strengths, hydrophilic surfaces, high surface metal diffusivity, and good conductivity, have been identified as a potential prospect for battery electrodes. In this study, taking a new 2D boron nitride allotrope, namely 2D orthorhombic diboron dinitride monolayer (o-B_2N_2) as representatives, we systematically explored several influencing factors, including electronic, mechanical, and their electrochemical properties (e.g., binding strength, ionic mobility, equilibrium voltage, and theoretical capacity). Considering potential charge-transfer polarization, we employed a charged electrode model to simulate ionic mobility and found ionic mobility has a unique dependence on the surface atomic configuration influenced by bond length, valence electron number, electrical conductivity, excellent ionic mobility, low equilibrium voltage with excellent stability, good flexibility, and extremely superior theoretical capacity, up to 8.7 times higher than that of widely commercialized graphite (3239.74 mAh g^{-1} Vs 372 mAh g^{-1}) in case of Li-ion batteries and 2159.83 mAh g^{-1} in case of Na-ion batteries, indicating that the new predicted 2D o-B_2N_2 monolayer possess the capability to be ideal flexible anode materials for Lithium and Sodium-ion battery. Our finding provides valuable insights for experimental explorations of flexible anode candidates based on 2D o-B_2N_2 monolayer.

1. Introduction

At present, the largest and most widespread energy storage technology available on the market consists exclusively of secondary batteries [1–3]. More specifically, rechargeable lithium-ion (LIB) batteries were extensively developed and implemented within electronic handheld systems as well as in electrical vehicles [4–6]. Nevertheless, the growing spread and the fast progress of E-vehicles and high-technology implementations like large-scale energy storage and so on, have led to a growing need for LIBs with relatively enhanced properties like a high-energy-density, a prolonged life-cycle, as well as an improved charge/discharge performance [7]. In this context, it is noteworthy that the materials used for negative/positive electrodes represent the primary constituents of batteries, which typically determine their electrochemical efficiency [8–10]. Since then, the research and understanding of new advanced and flexible high-capacity negative electrode materials remain the leading area of interest and development in this area [11,12]. Furthermore, beyond LIBs, other promising prospects as an energy storage medium consists of sodium-ion batteries (SIBs) owing to its reduced cost, safety, no-toxicity as well as its resourcefulness and reliability [13–15]. However, the further developments of acceptable high-efficiency electrodes suitable for NIBs represent another critical issue to be addressed likewise for LIBs.

Over the past decades, considerable attention was given to the development and exploitation of alternative negative electrode

* Corresponding authors.
E-mail addresses: wei.luo@physics.uu.se (W. Luo), rajeev.ahuja@physics.uu.se (R. Ahuja).

https://doi.org/10.1016/j.nanoen.2022.107066
Received 17 January 2022; Received in revised form 13 February 2022; Accepted 14 February 2022
Available online 25 February 2022

materials for LIB/SIB, resulting in remarkable breakthroughs. Within these versatile prospects, 2D materials were considered to be the most prospective alternative, due to their relatively large surface area as well as their outstanding physical/chemical features relative to their bulk counterparts, which can accommodate great electrochemical properties such as a very high energy densities [16–21]. In this regard, a wide range of 2D materials which include graphene [22–25], Borophene [26,27], α- and β-phase phosphorene [28–30], transition metal oxides/sulfides/carbonitrides as well as their associated composite structures were thoroughly explored prospectively through computational methods and experiment approaches to serve as potential anode materials for both Li/Na-ion batteries [11,31–34]. Notwithstanding, the majority of the identified 2D materials present relatively multiple limitations, including a limited specific capacity, a poor charge and discharge efficiency, instability and/or expensive manufacturing costs. Accordingly, further exploration and development of advanced 2D materials with improved electrochemical performance remains an important priority for both Li/Na-ion batteries.

While hexagonal boron nitride (h-BN) remains the most thoroughly investigated 2D material owing to its significant potential in nanoelectronics as a result of its indirect wide bandgap of 6 eV, [35–38] its non-performance derives also mainly from its large bandgap, given that the battery anode materials necessitate excellent electronic conductivity [39], the weak interaction between the alkali-metals and h-BN surface combined with insufficient Li-adsorption to convert its indirect large bandgap into a metallic nature additionally hampered its further applicability in energy storage applications [40,41]. Newly introduced by Demirci et al. (2020) [42], a new 2D polymorph of graphene-like boron nitride with the orthorhombic structural phase under the chemical formula o-B_2N_2 has been predicted through the density functional theory framework. In-depth investigations of the dynamic and mechanical stability showed that o-B_2N_2 monolayer is dynamically and mechanically stable. Additionally, the Ab-initio molecular dynamic computations revealed that o-B_2N_2 sustained its geometrical structure integrity up to 1000 K for 10 ps. The novel o-B_2N_2 being a semiconductor with a direct narrow bandgap of 0.64 eV opens up many new potential applications in energy conversion and storage, including photo-voltaic, rechargeable battery, and hydrogen storage. More crucially, considering that both Boron and Nitride belong to very light elements with a molecular weight of about 10.811 and 14.0067 a.u, respectively, it is expected that o-B_2N_2 could potentially reach an exceptional theoretical specific capacity for rechargeable lithium and sodium-ion batteries. Herein, we systematically explored for the first time the applicability of 2D o-B_2N_2 for both Li-ion and Na-ion battery electrode through the Density Functional Theory (DFT) framework and *ab-initio* molecular dynamic (AIMD) computations. We initially started our in-depth study by the structural geometry optimization and electronic properties of the new predicted o-B_2N_2 monolayer. Afterward, the binding strength of Lithium and Sodium at the possible suitable binding sites on the o-B_2N_2 surface were calculated using DFT and DFT-D3. The equilibrium voltage and theoretical capacity were investigated with a global optimization procedure based on the Basin-hopping Monte Carlo algorithm. The charge transfer, the deformation charge density after the adsorption of single Li/Na-atom were calculated and the ionic diffusion during Lithiation and Sodiation in o-B_2N_2 monolayer along with zigzag/armchair directions. A thorough comparison to other currently available 2D promising materials recently predicted for battery electrode, reveals that the new predicted 2D o-B_2N_2 monolayer can be distinguished as a potentially attractive addition to Lithium/Sodium-ion negative electrode materials with extremely high theoretical specific capacity and remarkably low ionic mobility.

2. Computational methods

Through our investigation, the geometrical structure, electronic, thermal, and mechanical stability, and electrochemical properties were explored through the framework of Density Functional Theory (DFT) as part of the Vienna Ab Initio Simulation Package (VASP) [43] code. The generalized gradient approximation in the form of Perdew Burke Ernzerhof (GGA-PBE) functional [44] were implemented self consistently within the framework of the projector augmented wave (PAW) by the plane-wave basis set with a kinetic-energy cutoff of 600 eV as a benchmark for all the further calculations based on the convergence criteria and the convergence criteria during the geometry optimizations were set to 10^{-6} eV and 10^{-3} eV/Å for energy and force, respectively. Furthermore, all the electronic structure calculations were performed through the optimal mixing parameters based on PBE-GGA ($\alpha = 0.0$) and the Heyd Scuseria Ernzerhof (HSE06) exchange–correlation hybrid functional which is mostly employed with a mixing parameter ($\alpha = 0.25$) and a screening parameter ($\mu = 0.20$) [45] were employed for better understanding of the electronic trend of the pristine material. During the geometry optimization of all structures, the vacuum layer was set to 20 Å in the z-direction to inhibit the interaction between stacked layers and periodic pictures. Based on the convergence test of E_{tot} Vs K-points, a large number of Monkhorst Pack K-point of about $8 \times 16 \times 1$ grid is adopted in the reciprocal space during the geometrical optimizations [46] in order to get very accurate properties. The charge transfer between atoms is evaluated on the basis of the Bader charge algorithm [47]. For the purpose of re-checking the thermal stability of the free-standing o-B_2N_2 monolayer obtained after full optimization, we perform the *ab-initio* molecular dynamics (AIMD) simulations in NVT ensemble with a time step of 2 fs for 10 ps at 800 K [48]. In addition, the Lithium and sodium ionic diffusion was investigated based on the CI-NEB approach [49] which requires the initial/final positions of Li/Na-diffusion as inputs and generates a number of intermediate states by linear interpolation. Subsequently, the minimum energy profile (MEP) between both states is calculated by minimizing the atomic forces in all images simultaneously subject to a harmonic coupling between neighboring images.

3. Results and discussion

Notwithstanding the considerable breakthroughs achieved, the drive to further design and identify improved 2D materials that provide superior battery performance is still at an initial stage of progress. The electronic conductivity of negative electrode material as the essential screening factor, although presents an interest within the study of charge/discharge performance has been poorly investigated so far [50–52]. A good conductivity in the negative electrode materials is required for electron transfer. Accordingly, the optimal suitable anode materials consist of semiconductors or highly conductive metallic conductors. Nevertheless, as the exploration of highly insulating materials as battery electrodes increases, more emphasis should be devoted to this aspect through theoretical and computational approaches.

The hexagonal boron nitride (h-BN) (Fig. 1(a,b)) with a graphene-like structure is the most extensively studied 2D materials owing to its prospective applicability within many versatile applications [37,38,53]. However, its ultimate suitability as a negative electrode material for rechargeable batteries is hampered due to the wide bandgap and limited electrochemical properties [39–41]. Therefore, we shall explore an alternative stable boron nitride structure formed through the geometrical rearrangement of B- and N-atoms with highly improved electrical conductivity and reveal its superlative electrochemical properties as an electrode in (Li^+,Na^+)-based ion batteries.

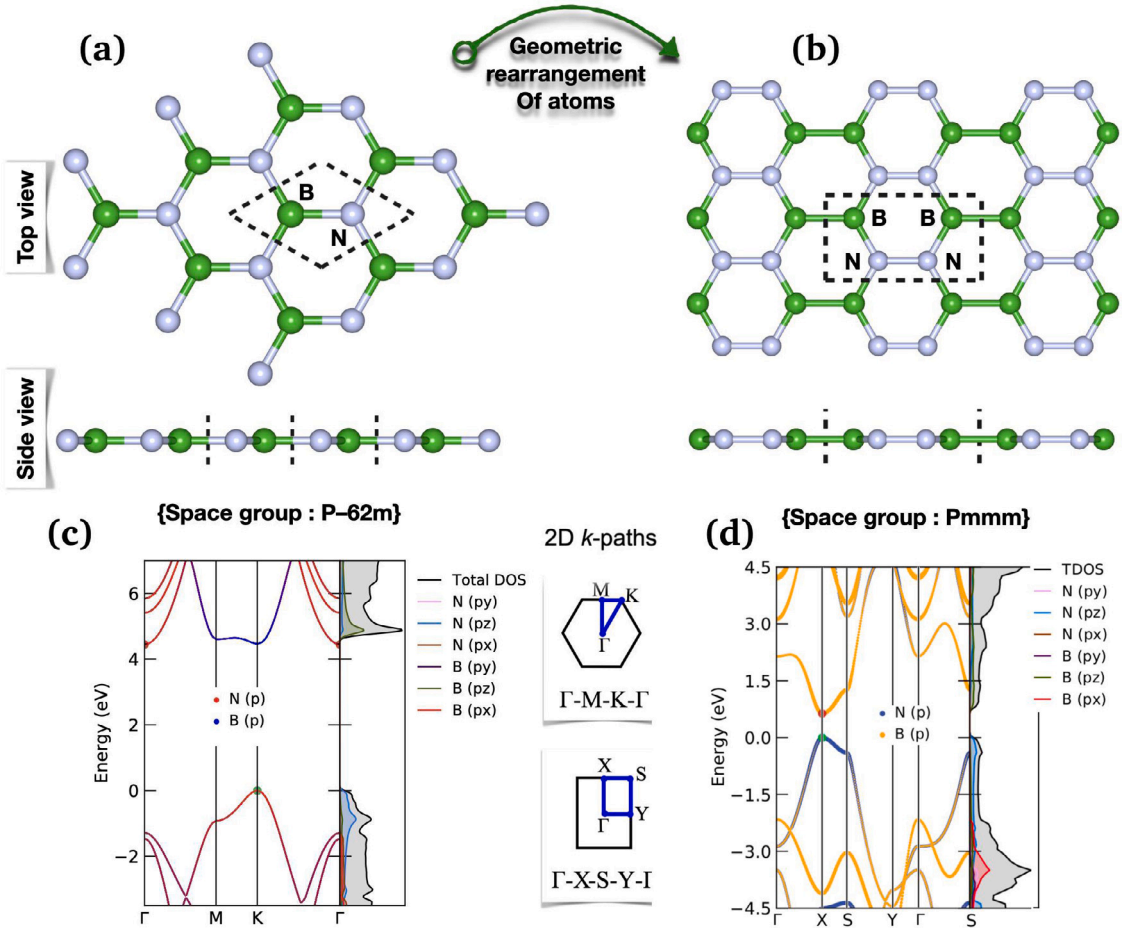

Fig. 1. Top and side views of a free-standing (a) h-BN and (b) o-B_2N_2 monolayers. The Projected band structure of both (c) h-BN and (d) o-B_2N_2 monolayers computed using GGA-PBE with corresponding projected density of state.

3.1. Structural and electronic properties

Currently reported for the first time by Dimiciri et al. [42] through DFT computations, Orthorhombic diboron dinitride with the chemical formula o-B_2N_2 is a new 2D material polymorph of boron nitride family with a planar honeycomb crystalline structure similar to that h-BN and graphene. Fig. 1(a, b, c, d) displays the top and side view of the fully optimized structure h-BN and o-B_2N_2 monolayers. The primitive cell of o-B_2N_2 is formed by four atoms built of alternating B–B, B–N, and N–N bonds. The optimized Bravais vectors of o-B_2N_2 are a = 4.570 Å and b = 2.496 Å, and the B–B, B–N, and N–N bond-lengths are 1.701 Å, 1.438 Å, and 1.438 Å respectively, which are in total agreement with previously reported studies.

To further understand the nature of the chemical bonds of o-B_2N_2 material and to characterize the localization of electrons in the interstitial spaces, the valence electron localization function were computed and depicted in Figure S1, the electron distributions are dominantly localized in the B–B, B–N, and N–N bonds compared to the hollow sites where the electron localization is near to zero. The present results indicate the covalent bonding characteristics in the o-B_2N_2 surface. For completeness, Bader charge analysis is carried out to elucidate the net charge at the boron and nitride atoms of about +0.907 $|e|$ and −0.907 $|e|$, respectively.

Based on the optimized lattice parameters, the electronic band structure with the corresponding projected density of states for both h-BN and o-B_2N_2 monolayers are calculated through GGA-PBE and HSE06 functional as shown in Fig. 1(e,f) and Figure S2. The obtained results revealed that the o-B_2N_2 is a semiconductor compound with an electronic bandgap of 0.647 eV much smaller than h-BN (4.446 eV). More specifically, Both the conduction band minimum (CBM) and the valence band maximum (VBM) are located at the Y-point, indicating that o-B_2N_2 is a direct semiconductor. Moreover, the CBM and VBM are mainly contributed by the pz-orbital of boron and nitride atoms.

3.2. Binding strength of lithium/sodium on o-B_2N_2onolayer

Typically, a prospective negative electrode material for (Li^+,Na^+)-based rechargeable batteries requires a comparatively significant binding strength of Lithium/Sodium as a fundamental prerequisite. Accordingly, We shall first compute the binding strength of a single Li^+/Na^+ on different possible binding sites of o-B_2N_2 monolayer through both DFT and DFT-D3 methods. A large super-cell of about 2 × 3 × 1 was adopted during the Li/Na-intercalation process to inhibit the interactions between neighboring Li/Na-ions on o-B_2N_2 surface. Owing to D_{2h} symmetry of the o-B_2N_2 monolayer, Seven potential binding sites were assumed at the beginning of the computations, which can be categorized into three categories denoted by H (hollow), B (Bridge), and *T* (top) as depicted in Fig. 2(a). The first one contains, H1 and H2 located above the hollow site for B_4N_2- and B_2N_4-Hexagon, respectively, the second category contains TB and TN positioning on the top of any B- and N-atom based on crystal symmetry, and the third category holds the B1, B2, B3 positioning between B–B and N–N, B–N bonds, respectively. The principle which consists in recognizing the privileged binding site of Li/Na-atom on o-B_2N_2 surface is derived according to the binding strength equation given formerly through of DFT and DFT-D3:

$$E_b = E_{(Li,Na)@B_4N_2} - E_{B_2N_2} - E_{(Li,Na)} \quad (1)$$

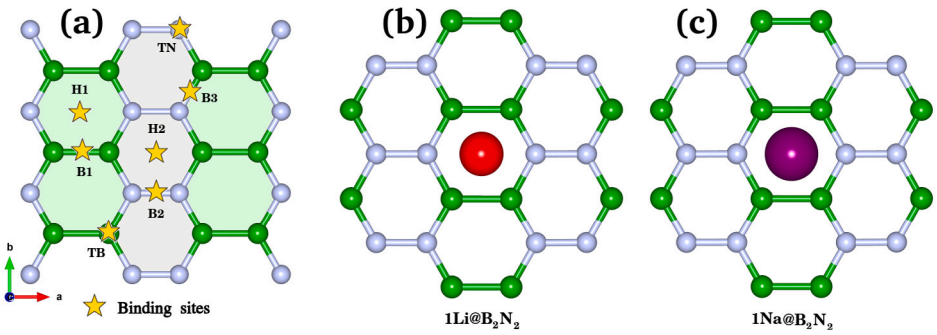

Fig. 2. (a) The suitable binding sites for Li and Na on the free-standing o-B_2N_2 monolayer (TN/TB refers to the binding sites at the top of N/B atoms; H1 and H2 denote the hollow-sites of the hexagonal B_4N_2-ring and B_2N_4-ring, respectively; B1, B2, and B3 denotes the binding sites at the B–B, N–N, and B–N bridges, respectively). (b,c) The top views of the most stable optimized configuration of single Li and Na atom adsorbed on the o-B_2N_2 monolayer.

Table 1
Binding strength using DFT and DFT-D3, binding height, charge transfer Q (|e|), and work function of Lithium/Sodium adsorbed on the most favorable binding site.

Systems	Binding site	E_b^{DFT} (eV)	E_b^{DFT-D3} (eV)	h (Å)	$Q_{Li/Na}$ (|e|)	WF (eV)
B_2N_2@Li	H1	−1.274	−1.408	1.674	+0.787	3.363
	H2	−0.966	−1.097	1.708	+0.835	3.397
B_2N_2@Na	H1	−0.435	−0.569	2.190	+0849	3517
	H2	−0.357	−0.452	2.228	+0872	3491

Wherein $E_{(Li,Na)@B_4N_2}$ and $E_{B_2N_2}$ refers to the energies of the o-B_2N_2 super-cell after and before the adsorption of single Li^+/Na^+, respectively, $E_{(Li,Na)}$ represents the average energy of Li/Na-atom in bulk reference state. By definition, the more the binding strength is negative, more the binding configuration is more stable, indicating the scattering distribution of the adsorbed Li/Na-atoms instead of their clustering, Therefore, avoiding the issues arising from the formation of metal-dendrites or metal-clusters (e.g. short circuits) during charge/discharge process. Within the binding sites examined, it is observed that H1 and H2 sites exhibit the lowest binding strength for both Li and Na metals and the remaining adsorption sites have deviated to the H1 or H2 positions. Table 1 summarize the computed binding strength using DFT and DFT-D3 functionals, binding height, charge transfer, and work function for the first two most stable binding sites. It can be distinguished that the H1 exhibits the lowest binding strength of about −1.408 and −0.569 eV for both Li and Na atoms, respectively (Fig. 2(b,c) represent the full geometry optimization of Li/Na atom at H1-site). These binding strength are much large compared to recently reported 2D materials, including h-BP (−0.202/−0.160 eV) [54,55], h-BN (−0.275 eV for Li) [40,41]and Borophosphene o-B_2P_2 (−1.06 eV for Li) [56]. This reveals a more rapid charging process with a more extensive binding interaction occurring between orthorhombic B_2N_2 and Li/Na atom versus the weak binding to metal ions in the hexagonal boron nitride monolayer [40]. More significantly, these findings suggest a uniform spread of Li/Na atoms on the o-B_2N_2 surface throughout the intercalation mechanism instead of gathering up to form metal-dendrites, providing ensure better reversibility as well as a significant benefit in the stability and safety of advanced (Li^+,Na^+)-based rechargeable batteries.

3.3. Record-high Li/Na-storage capacity and equilibrium voltage

To further explore the electrochemical performance of o-B_2N_2 as an anode material of (Li^+,Na^+)-based ion batteries, the record-high theoretical specific capacity, and the equilibrium potential voltage were investigated by step-wise inserting Li- and Na-ions onto both sides of the o-B_2N_2 surface. Given that the H1- and H2-sites were the more energetically stable binding sites. At first, Li/Na-atoms have uniformly inserted at the H1-sites on either side of o-B_2N_2 surface until the full recovery is reached forming the first Li-layer, and subsequently, Li/Na-atoms were placed at H2 by forming the second Li-layer, thereby a sequence of intermediate configurations under the chemical formula of $(Li,Na)_n@B_2N_2$ (n = 0.5, 1.0, 1.5, 2.0, 2.5, 3.0) are taken into consideration. The average binding strength E_b^{Avg} of n(Li,Na)-atoms adsorbed on both sides of o-B_2N_2 monolayer are computed through the formula:

$$E_b^{Avg} = (E_{(Li,Na)_n@B_2N_2} - E_{B_2N_2} - n\mu_{(Li,Na)})/n \quad (2)$$

where $E_{(Li,Na)_n@B_2N_2}$ and $E_{B_2N_2}$ refers to the total energy of $(Li,Na)_b@B_2N_2$, B_2N_2 respectively. The $\mu_{(Li,Na)}$ represent the chemical potential of Li and Na-atom. The red line in Fig. 3(a,b) depict the average binding strength of $(Li,Na)_n@B_2N_2$ and the corresponding fully optimized structure for each configuration are illustrated in Figure S3 and S4. One can notice the binding strength $Li_n@B_2N_2$ are higher than those obtained in $Na_n@B_2N_2$ which is principally attributed to the decrease of the electrostatic interaction of (Li, Na)-atoms with the o-B_2N_2 anode material as well as to the reinforced repulsion of the (Li, Na)-atoms at relatively higher concentrations. Moreover, the binding energies of all configurations throughout the charging mechanism remain negative, thus avoiding the formation of (Li, Na) dendrites. Accordingly, the o-B_2N_2) anode for (Li, Na)-ion batteries could store a maximum of 36 Li ($Li_3@B_2N_2$) and 24 Na ($Na_2@B_2N_2$).

One further crucial element for evaluating the high-efficiency of (Li^+,Na^+)-based ion batteries is the potential voltage. Conceptually, the process of lithiation/delithiation (sodiation/desodiation) of the battery electrode can be considered as the half-cell reaction of (Li, Na)-anode, as:

$$(Li,Na)_{x_1}@B_2N_2 + (x_2 - x_1)(Li^+, Na^+) + (x_2 - x_1)e^- \rightleftharpoons (Li,Na)_{x_2}@B_2N_2 \quad (3)$$

The battery open-circuit voltage at each equilibrium stage of the reaction (3) can be estimated through a direct thermodynamic calculation of the Gibbs free energy ($\Delta_r G(x)$) using the Nernst formula given below:

$$V(x) = -\frac{\Delta_r G(x)}{n.F} \quad (4)$$

With the Gibbs free-energy $\Delta_r G(x)$ given as:

$$\Delta_r G(x) = -\frac{1}{n_{B_2N_2}}\frac{\partial G(x)}{\partial x} \quad (5)$$

where F, $n_{B_2N_2}$ and G(x) refers respectively to the Faraday constant, the number of moles in the o-B_2N_2 material and the Gibbs free energy at stage x. In the case of the solid-state where the volume, pressure, and entropy effects at ambient temperature were negligible, the G(x) in Eqs. (4) and (5) is commonly estimated with the total electronic energy of the systems at each stage, expected to be the main terms of the free energy of reaction at equilibrium, which leads to:

$$V(x) \approx -\frac{E_{(Li,Na)_{x_2}@B_2N_2} - E_{(Li,Na)_{x_1}@B_2N_2} - (x_2 - x_1)\mu_{(Li,Na)}}{(x_2 - x_1)} \quad (6)$$

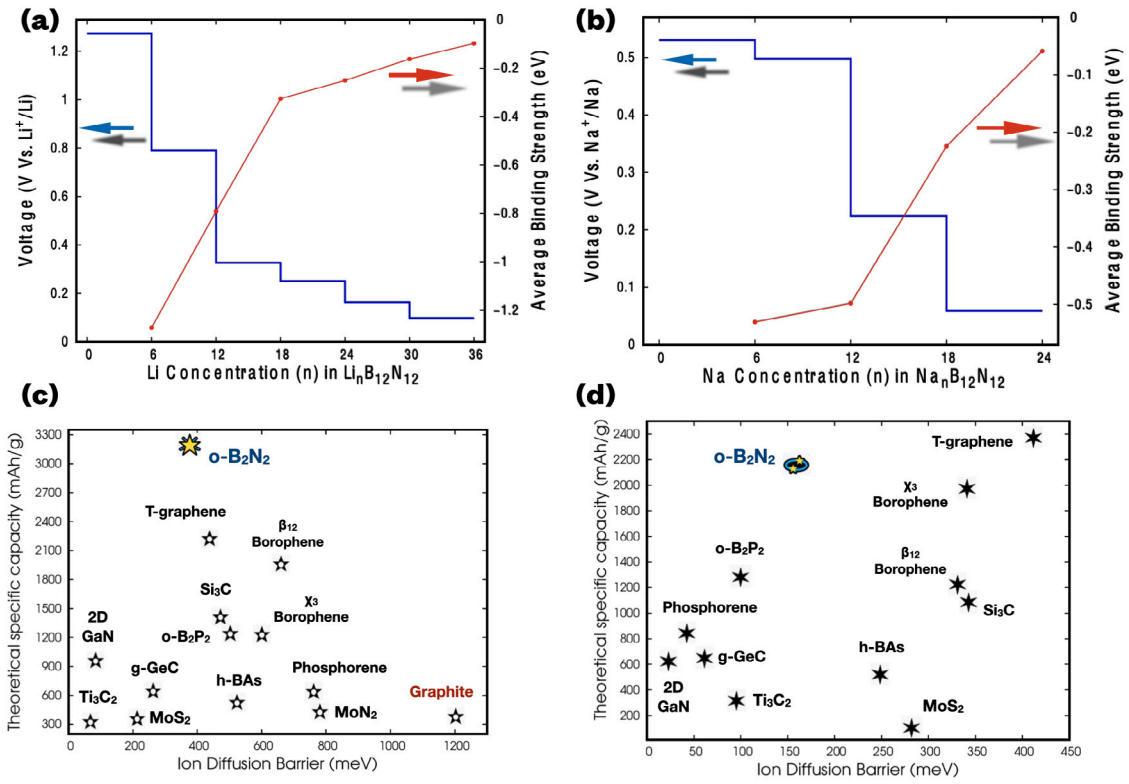

Fig. 3. (a,b) The voltage profiles (V) with average binding strength (eV) as a function of the Li- and Na-concentration (n) in $(Li/Na)_nB_2N_2$, respectively. (c,d) A Comparison of the theoretical specific capacity with the some previously potential 2D anode materials.

where $E_{(Li,Na)_{x_1}@B_2N_2}$ and $E_{(Li,Na)_{x_2}@B_2N_2}$ refers to electronic total energies of x_1 and x_1 (Li, Na)-atoms adsorbed on both sides of o-B_2N_2 surface, respectively. The blue line in Fig. 3(a,b) illustrates the open-circuit voltage as a function of the (Li, Na)-concentrations x in $(Li,Na)_x@B_2N_2$ systems. It can be noticed that all the average open-circuit voltages are positive, which confirms the applicability of o-B_2N_2 monolayer as a negative electrode for both Li/Na-ion batteries. Also, one can notice that as the (Li,Na)-concentration increase, the open-circuit voltage displays a declining tendency through six (Li) and four (Na) insertion potential plateaus with an average voltage of about 0.483 V Vs Li^+/Li and 0.328 V Vs Na^+/Na. Such moderate average voltages are in the desirable range for achieving maximum power density through the charge/discharge process and can effectively prevent the formation of (Li, Na)-dendrites providing improved stability of the battery electrode. Hence, the o-B_2N_2 monolayer could serve as a high-performance prospective anode for (Li^+,Na^+)-ion batteries.

According to these findings, the highest theoretical specific capacity (C_{th}) of B_2N_2 anode material for (Li^+, Na^+)-storage can be derived through the formula below:

$$C = \frac{x_{max}.z.F}{W_{B_2N_2}}.10^3 \quad (7)$$

where x_{max} and z are to the maximum (Li^+, Na^+)-concentrations and the valence state of fully ionized Li/Na. he $W_{B_2N_2}$ is the molecular weight of o-B_2N_2 monolayer. Accordingly, the derived theoretical specific Li^+ and Na^+ storage capacity on the B_2N_2 anode material are about 3239.74 and 2159.83 mAh g^{-1}, respectively.

Furthermore, it is extremely worthwhile to highlight the ultra-high (Li^+, Na^+)-storage capacity of this newly introduced Boron Nitride polymorph (o-B_2N_2) monolayer. A comparison of the storage capacity of o-B_2N_2 with some typical 2D anode materials for (Li^+, Na^+)-ion batteries are illustrated in Fig. 3(c,d). One can clearly notice that the majority of the recent identified 2D anode materials possess a Li^+-storage capacity of less than 1000 mAh g^{-1} [15,29,57–63], which is approximately 3–8 times smaller than that obtained in this work for the o-B_2N_2 anode material (3239.74 mAh g^{-1}). In addition, a few 2D anode materials present a relatively high Li^+-storage capacity of over 1000 mAh g^{-1} [27,64–67]. In particular, T-graphene monolayer recently reported by Zhang, Xiaoming, et al. [67], exhibits the maximum Li^+-storage capacity of 2233.2 mAh g^{-1}. Nevertheless, the Li^+-storage capacity of o-B_2N_2 can exceed that of T-graphene with up to 1006,54 mAh g^{-1}. A new high-record of Li^+-storage capacity in 2D battery electrode is reached by the o-B_2N_2 monolayer. Further, for the purpose of comparison, we likewise display in a red star shape in Fig. 3(c) the output of the widely studied and commercialized graphite anodes [68,69], in which the Li-storage capacity of the o-B_2N_2 is up to 8.7 times higher of that of graphite (3239.74 mAh g^{-1} Versus 372 mAh g^{-1}). In case of Na-ion batteries, as depicted in Fig. 3(d), the Na^+-storage capacity of o-B_2N_2 monolayer with 2159.83 mAh g^{-1} is moderately lower than that of T-graphene of about 2357.2 mAh g^{-1} and significantly larger than those of well-known 2D materials [15,27,57–61,64–67].

3.4. Charge transfer and diffusion kinetics during lithiation/sodiation

High-performance (Li^+,Na^+)-based rechargeable batteries development is critically dependent on the capability of the negative electrode materials especially on the charge/discharge process, which is typically driven by the kinetic properties of electron transfer. Accordingly, the charge density difference of Li/Na atom adsorbed at the most favorable site on o-B_2N_2 monolayer was examined by means of the equation yielded below:

$$\Delta\rho = \rho_{M@B_2N_2} - \rho_{B_2N_2} - \rho_M \quad (M = Li, Na) \quad (8)$$

where $\rho_{B_2N_2}$ and $\rho_{M@B_2N_2}$ are the electron charge density of o-B_2N_2 monolayer before and after the adsorption of Li/Na atom, respectively, and ρ_M represents the electron charge density of single Li/Na atom isolated in the system by keeping the same structural parameters without any further geometrical optimization. Fig. 4(a,b) illustrates the

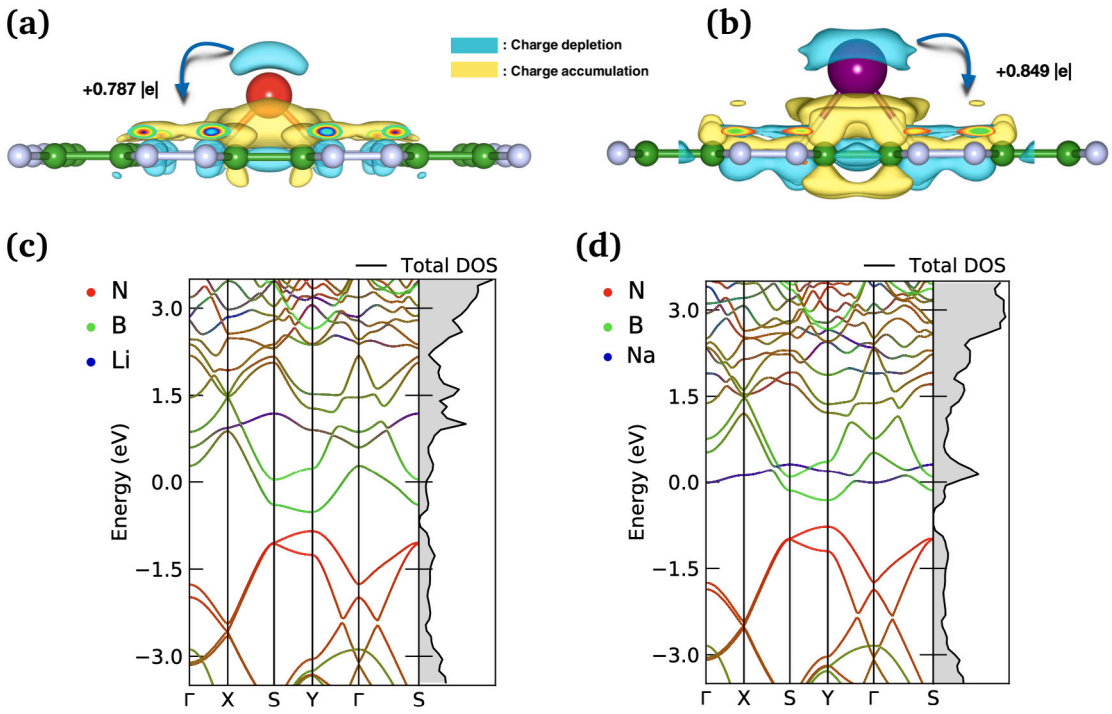

Fig. 4. (a,b) Side view of difference charge density ($\Delta\rho$) for Li- and Na-atom adsorbed at the most stable binding site (H1) on o-B_2N_2 surface, respectively. The Yellow and cerulean refer to the electron accumulation and depletion, respectively, and the charge transfer from the Li- and Na-atom to o-B_2N_2 surface are about 0.787 and 0.849 $|e|$. (c,d) The Projected band structure with a corresponding total density of state for 1Li@B_2N_2 and 1Na@B_2N_2 systems, respectively.

depletion and accumulation of charges for both systems represented as 3D isosurface distributed charge density plots. One can notice that the charge accumulating zone represented by the yellow color is situated within the Li/Na atom and the surface of the o-B_2N_2 material, and the depletion of charge represented by the blue-light color surrounds the Li/Na atom, which indicating that the Li/Na atom considered donated charge to the o-B_2N_2 monolayer, which results in the higher electronegativity of Boron and Nitride atoms versus to that of Li/Na atoms. Moreover, the charge transfer approach was performed using the Bader charge algorithm and the results are summarized in the Table 1. It can be noticed that each single Li and Na loses an average electron-charge of about 0.787 and 0.849 $|e|$, respectively.

Additionally, a more deep understanding of the binding process and the electronic behavior after the adsorption of a single Li/Na atom were surveyed through the computation of the projected electronic band structure with the corresponding total density of state, as shown in Fig. 4. Our findings clearly indicate the systems change the electronic behavior from a semiconductor to metallic states after a single Li/Na-binding with an explicit contribution of Li/Na atom near to Fermi-level, ensuring much enhanced electrical conductivity and a fast transfer of electrons in the anode throughout the full adsorption and desorption process, which fulfills a key role in the high throughput capacity of (Li^+,Na^+)-based ion batteries.

Besides the electronic conductivity, Li/Na ion diffusion in the anode material represents another vital parameter that affects the electrochemical performance of the battery, especially during high charge/discharge processes [51,52]. Therefore, the dilute Li- and Na-ion diffusion pathways with their corresponding minimum energy profile (MEP) were estimated through the CI-NEB approach. The top view of the fully optimized three scattering pathways (I, II, III) explored in this work and their corresponding relative energy profile are illustrated in Fig. 5. The three typical considered pathways consist of a Li-, and Na-ion migration along the a-direction (Zigzag) refers to the path I and b-direction (armchair) refers to path II and Path III over the H2-site of o-B_2N_2 monolayer described as follow:

- Path I imply that the Li–Na-ion diffuse along the b-direction perpendicular to the directions of B–B and N–N bonds with a computed minimum energy barrier of about 0.47 and 0.16 eV, respectively.
- Path II involves that the Li- and Na-ion diffuse from the more stable binding site with the highest binding energy (H1) to the nearest H1 along the a-direction in parallel to B–B and N–N bonds. One can notice that the Li- and Na-ion have to overcome an energy barrier of 0.38 and 0.27 eV, respectively.
- Path III suggests that Li- and Na-ion are scattering over the H2 site with a computed minimum energy profile of 0.39 and 0.28 eV, respectively.

The estimated energy barrier values are in accordance with the results of binding energy summarized in Table 1, the Li-ion diffusion barrier in path II present the lowest energy profile as compared to other paths (II and III), while the Na-ion migration barrier in the path I exhibit the lowest energy of about 0.16 eV. For comparison purposes, the calculated minimum diffusion barriers of Li- and Na-ion on o-B_2N_2 surface are similar and comparable to those recently identified 2D materials as illustrated in Fig. 3(c,d), including o-B_2P_2 monolayer (500/100 meV for Li/Na) [64,65], Si_CC monolayer (470/340 meV for Li/Na) [66], h-BAs monolayer (522/248 meV for Li/Na) [57] and T-graphene with energy barrier of about 440/410 meV for Li/Na [67] and so on [15,60,63,70–73].

In addition, the partially and fully lithiated/sodiated process were explored through the electron localization functions (ELF), which refers by definition to the Jellium-like homogeneous electron-gas with the value range between 0.00 and 1.00. Whereas the 1.00 (0.50) represents completely localized (delocalized) electrons, while 0.00 refers to a very low charge density. The Fig. 6 depict the electron localization function (ELF) of the partially ($Li_2B_2N_2$) and fully ($Li_3B_2N_2$) lithiated systems. One can be clearly observed from Fig. 6(a), a great localization of charge between Li atoms in the second Li-layer and the electron transfer is occurring from the 2nd to the 1st Li-layer with an average charge transfer calculated through the Bader-charge algorithm and

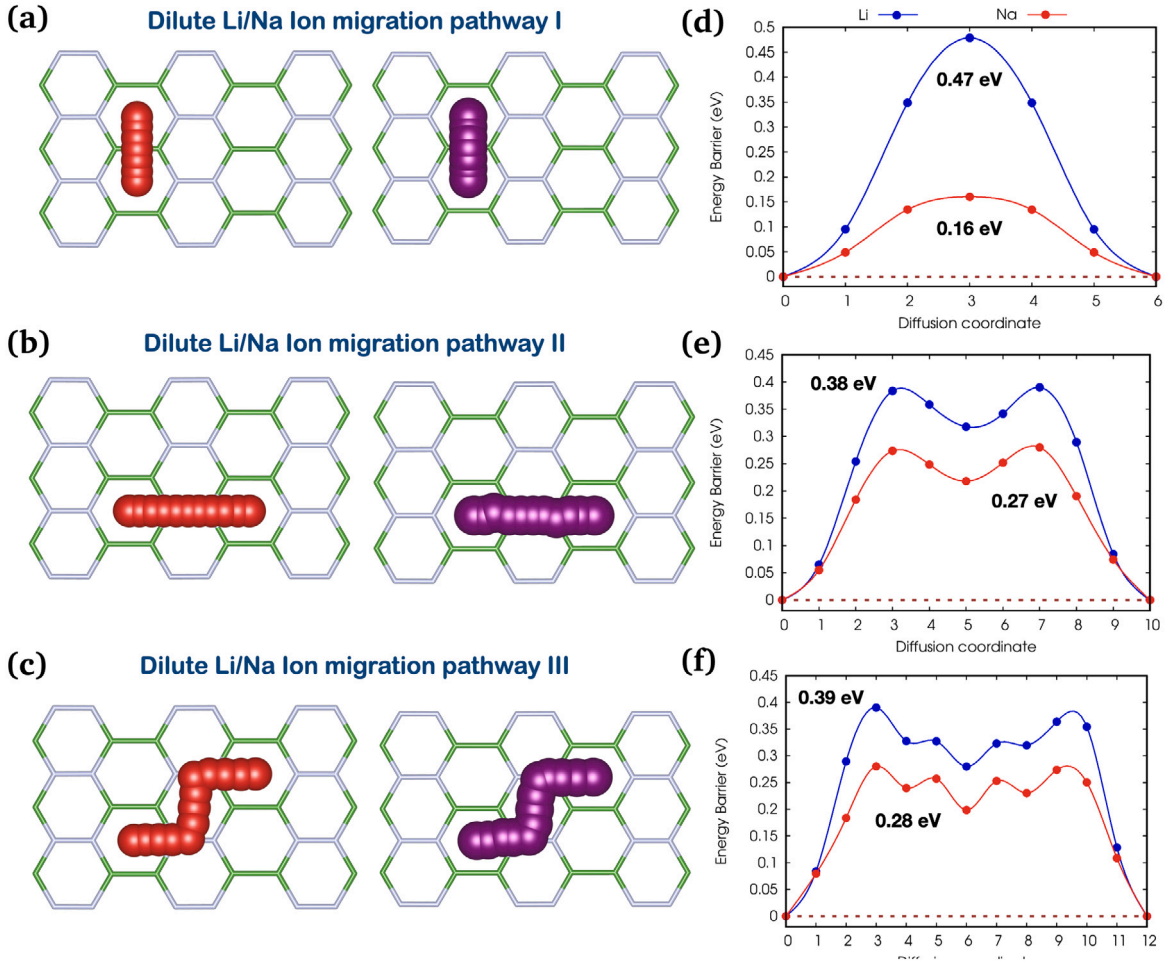

Fig. 5. Dilute Li/Na ion diffusion pathways on o-B_2N_2 surface. (a,b,c) The top view of the full optimized three various Li/Na-ion diffusion pathways (I, II, and III). (e,f,g) The corresponding minimum energy barriers for Li- and Na-ion along the three pathways.

Table 2
Estimated average charge transfer through Bader charge analysis for o-B_2N_2 monolayer and its partially and fully lithiated/sodiated states.

Systems	Average charge state ($\|e\|$)		
	Li/Na	B	N
o-B_2N_2	–	+0.907	−0.907
$Li_1B_2N_2$	+0.557	+0.852	−1.409
$Li_2B_2N_2$	+0.537	+0.935	−1.472
$Li_3B_2N_2$	+0.453	+0.914	−1.367
$Na_1B_2N_2$	+0.382	+1.054	−1.436
$Na_2B_2N_2$	+0.317	+1.158	−1.475

summarized in Table 2. In addition, a similar trend is observed in the case of an extra Li-layer adsorbed on the systems as illustrated in Fig. 6(b). The 2nd and 3rd Li-layer serves like an electron-donor with average charge transfer of about 0.507 and 0.68 $|e|$.

3.5. Additional comment on the stability of o-B_2N_2uring lithiation/sodiation

During the lithiation and sodiation process, the anode materials can be subject to a considerable expansion with the possibility of pulverization, which can cause a rapid decrease in their capacity and a reduced cycle-life. In this context, we have checked the mechanical and thermal stability of o-B_2N_2 during lithiation and Sodiation. First, the elastic properties of o-B_2N_2 monolayer were explored through the energy-strain approach implemented in the VASPKIT package [74] in which the stiffness tensor is derived from the second-order derivative of the total energies as the respect of applying strain between −2.0% and +2.0% in steps of 0.50%. The elastic strain energy per unit area is expressed using Voigt notation and can be expressed by the following expression:

$$U(\epsilon_x, \epsilon_y) = \frac{1}{2}C_{11}\epsilon_x^2 + \frac{1}{2}C_{22}\epsilon_y^2 + C_{12}\epsilon_x\epsilon_y \quad (9)$$

With ϵ_x and ϵ_y refers to the uni-axial strain along the x- and z-direction, respectively. The elastic constants $C_{11} \neq C_{22}$ owing to the anisotropy of the o-B_2N_2 monolayer. The computed elastic constants are fulfilling the strict mechanical stability criteria as defined by $C_{11} > 0$, $C_{22} > 0$, $C_{66} > 0$, and $C_{11}.C_{22} - C_{12}^2 > 0$. As summarized in Table 3, the C_{11} = 250.391 N/m, C_{12} = 35.105 N/m, C_{22} = 291.646 N/m, and C_{66} = 21.976 N/m, which are slightly comparable to those of h-BN and significantly greater than those of orthorhombic borophosphorene (o-B_2P_2), hexagonal boron phosphide (h-BP). Moreover, the mechanical properties are described in terms of the in-plane Young's modulus and Poisson's ratio along the x- and y-directions and calculated through the formulas:

$$Y_x = \frac{C_{11}C_{22} - C_{12}C_{21}}{C_{22}}, \quad Y_y = \frac{C_{11}C_{22} - C_{12}C_{21}}{C_{11}} \quad (10)$$

$$\nu_x = \frac{C_{12}}{C_{22}}, \quad \nu_y = \frac{C_{12}}{C_{11}} \quad (11)$$

The calculated in-plane Young's modulus in the x- and y-direction are about 246.165 N/m and 286.724 N/m, respectively. While the Poisson's ratio is calculated to be ν_x = 0.12 and ν_y = 0.12. These

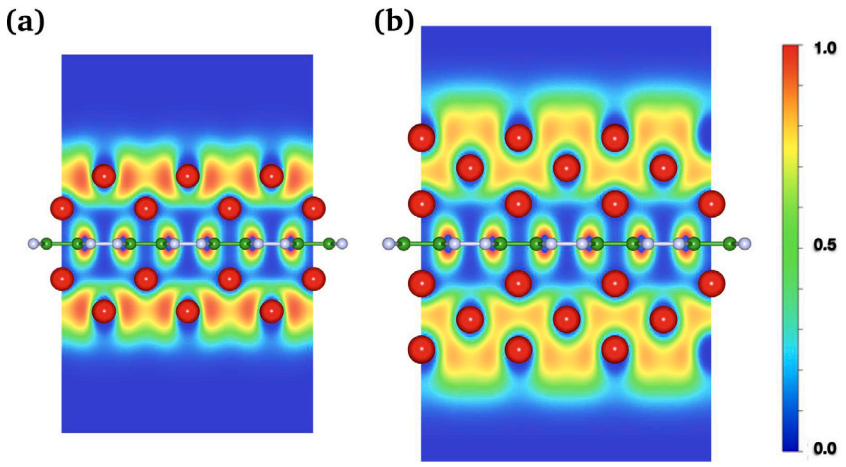

Fig. 6. The valence Electron localization function (ELF) map of o-B_2N_2 monolayer with (a) two Li-layers and (b) three Li-layers.

Table 3
A comparative summary of calculated elastic constants for different 2D materials.

2D materials	Elastic constants (N/m)			
	C11	C12	C22	C66
o-B_2N_2	250.391	35.105	291.646	21.976
B_2N_2@Li	253.165	39.173	280.058	23.170
B_2N_2@Na	253.279	40.199	274.347	23.112
o-B_2P_2 [64]	154.4	34.7	135.7	49.6
h-BN [78]	290.2	64.4	290.2	–
h-BP [78]	145.5	38.8	145.5	–
Graphene [78]	351.6	64.10	351.6	–

findings are in agreement with the previous work and significantly comparable to those obtained in the h-BN monolayer [42]. As compared to some other 2D materials, these results are significantly greater than those of hexagonal and orthorhombic boron phosphide [64,75], black phosphorene [76], but smaller than those of graphene monolayer [77].

Additionally, It is important to point out that the thermal stability of the electrode during the charge/discharge process represents another main factor for high-performance batteries. In this context, the AIMD simulations were carried out at 300 K and a time scale of about 10 ps for both $Li_3B_2N_2$ and $Na_2B_2N_2$ systems as displayed in Figure S6 and S7. It can be clearly remarked from the screenshot of the resulting structures that both systems remain the same geometrical arrangement without any structural deformations. Also, the corresponding variation of total energy and temperature as a function of a time scale is incredibly small, which indicate great thermal stability of $Li_3B_2N_2$ and $Na_2B_2N_2$ at 300 K. All these findings reveal excellent mechanical and thermal stability of o-B_2N_2 monolayer during the charge/discharge process, suggesting an exceptionally promising prospect for a flexible electrode in next-generation batteries.

4. Conclusions

To conclude, we have revealed for the first time the superlative electrochemical properties of 2D o-B_2N_2 as flexible anode for (Li^+,Na^+)-based ion batteries through several influencing factors based on the density functional theory calculations and *ab-initio* molecular dynamics simulations. The binding strength, kinetics as well as the ionic-mobility of Li^+ and Na^+ intercalation were thoroughly evaluated. The finding indicates that the Li- and Na atoms can be stably inserted into B_2N_2 surface without clustering and tend to be preferably adsorbed at the B_4N_2-hollow site with a binding strength of about −1.408 and −0.569 eV, respectively. Additionally, the o-B_2N_2 provides outstanding electronic conductivity throughout the partial lithiation/sodiation process, a critical feature required for its application as a battery electrode. The high Li^+ and Na^+ storage capacity in both sides of o-B_2N_2 surface can achieve a very high-record theoretical specific capacity of about 3239.74 and 2159.83 mAh g^{-1}, respectively. This represents a new superior record for Li^+-storage and significantly higher compared to many other 2D materials for Na^+-storage. Also, these extremely high lithiated/sodiated exhibits good mechanical and thermal stability. Besides, the comparatively low open-circuit voltages of approximately 0.48 V (Li) and 0.33 V (Na) and Li/Na-ionic mobility of about 0.38 and 0.16 eV, respectively, provide a significant advantage in the high-performance Li- and Na-ion batteries. Based on the above remarkable electrochemical properties, it can be expected that 2D o-B_2N_2 offers a great prospect to be used as a new battery electrode for Li and Na ion batteries. Therefore, it is highly believed and hopefully, the present work can serve as a guideline for both computational and experimental discussions on the promising and versatile 2D anode materials.

CRediT authorship contribution statement

Nabil Khossossi: Conceptualization, Data curation, Formal analysis, Investigation, Methodology, Validation, Visualization, Writing – original draft, Writing – review & editing. **Wei Luo:** Conceptualization, Formal analysis, Validation, Visualization, Writing – review & editing. **Zakaryae Haman:** Conceptualization, Formal analysis, Visualization, Validation, Writing – review & editing. **Deobrat Singh:** Conceptualization, Formal analysis, Visualization, Validation, Writing – review & editing. **Ismail Essaoudi:** Conceptualization, Formal analysis, Validation, Writing – review & editing. **Abdelmajid Ainane:** Conceptualization, Formal analysis, Validation, Writing – review & editing. **Rajeev Ahuja:** Conceptualization, Formal analysis, Funding acquisition, Project administration, Resources, Software, Supervision, Validation, Writing – review & editing.

Declaration of competing interest

The authors declare that they have no known competing financial interests or personal relationships that could have appeared to influence the work reported in this paper.

Acknowledgments

We gratefully acknowledge computational resources from the Swedish National Infrastructure for Computing SNIC (2021/1- 42) and HPC2N. I.E and A.A. acknowledge the PPR2 project: (MISTERSFC-CNRST). N.K., W.L., D.S. and R.A. thanks the Swedish Research Council (VR-2016- 06014 & VR-2020-04410) and J. Gust. Richert stiftelse, Sweden (2021-00665) for financial support.

Appendix A. Supplementary data

Supplementary material related to this article can be found online at https://doi.org/10.1016/j.nanoen.2022.107066.

- Electron localization function (ELF) of 2D o-B_2N_2, electronic band structure of h-BN and o-B_2N_2 using HSE-06.
- Different stable configurations of Li- and Na-atoms adsorbed on o-B_2N_2 surface with corresponding electronic band structures.
- Ab-initio Molecular Dynamics simulations for $Li_3B_2N_2$ and $Na_2B_2N_2$.

References

[1] Y. Sun, N. Liu, Y. Cui, Promises and challenges of nanomaterials for lithium-based rechargeable batteries, Nat. Energy 1 (7) (2016) 1–12.
[2] X.-B. Cheng, R. Zhang, C.-Z. Zhao, Q. Zhang, Toward safe lithium metal anode in rechargeable batteries: a review, Chem. Rev. 117 (15) (2017) 10403–10473.
[3] Y. Bahari, B. Mortazavi, A. Rajabpour, X. Zhuang, T. Rabczuk, Application of two-dimensional materials as anodes for rechargeable metal-ion batteries: A comprehensive perspective from density functional theory simulations, Energy Storage Mater. (2020).
[4] W. Liu, M.-S. Song, B. Kong, Y. Cui, Flexible and stretchable energy storage: recent advances and future perspectives, Adv. Mater. 29 (1) (2017) 1603436.
[5] G. Harper, R. Sommerville, E. Kendrick, L. Driscoll, P. Slater, R. Stolkin, A. Walton, P. Christensen, O. Heidrich, S. Lambert, et al., Recycling lithium-ion batteries from electric vehicles, Nature 575 (7781) (2019) 75–86.
[6] J.W. Choi, D. Aurbach, Promise and reality of post-lithium-ion batteries with high energy densities, Nat. Rev. Mater. 1 (4) (2016) 1–16.
[7] A. Manthiram, A reflection on lithium-ion battery cathode chemistry, Nature Commun. 11 (1) (2020) 1–9.
[8] K. Takada, T. Inada, A. Kajiyama, H. Sasaki, S. Kondo, M. Watanabe, M. Murayama, R. Kanno, Solid-state lithium battery with graphite anode, Solid State Ion. 158 (3–4) (2003) 269–274.
[9] R. Mukherjee, R. Krishnan, T.-M. Lu, N. Koratkar, Nanostructured electrodes for high-power lithium ion batteries, Nano Energy 1 (4) (2012) 518–533.
[10] M. Singh, J. Kaiser, H. Hahn, Thick electrodes for high energy lithium ion batteries, J. Electrochem. Soc. 162 (7) (2015) A1196.
[11] D. Singh, V. Shukla, N. Khossossi, A. Ainane, R. Ahuja, Harnessing the unique properties of MXenes for advanced rechargeable batteries, J. Phys.: Energy 3 (1) (2020) 012005.
[12] N. Khossossi, D. Singh, A. Ainane, R. Ahuja, Recent progress of defect chemistry on 2D materials for advanced battery anodes, Chem.–Asian J. 15 (21) (2020) 3390–3404.
[13] C. Hakim, N. Sabi, I. Saadoune, Mixed structures as a new strategy to develop outstanding oxides-based cathode materials for sodium ion batteries: A review, J. Energy Chem. (2021).
[14] H.S. Hirsh, Y. Li, D.H. Tan, M. Zhang, E. Zhao, Y.S. Meng, Sodium-ion batteries paving the way for grid energy storage, Adv. Energy Mater. 10 (32) (2020) 2001274.
[15] N. Khossossi, A. Banerjee, I. Essaoudi, A. Ainane, P. Jena, R. Ahuja, Thermodynamics and kinetics of 2*D* g-GeC monolayer as an anode materials for Li/Na-ion batteries, J. Power Sources 485 (2021) 229318.
[16] K. Khan, A.K. Tareen, M. Aslam, A. Mahmood, Y. Zhang, Z. Ouyang, Z. Guo, H. Zhang, et al., Going green with batteries and supercapacitor: Two dimensional materials and their nanocomposites based energy storage applications, Prog. Solid State Chem. 58 (2020) 100254.
[17] J. Lin, T. Yu, F. Han, G. Yang, Computational predictions of two-dimensional anode materials of metal-ion batteries, Wiley Interdiscip. Rev.: Comput. Mol. Sci. 10 (5) (2020) e1473.
[18] Y.-M. Chang, H.-W. Lin, L.-J. Li, H.-Y. Chen, Two-dimensional materials as anodes for sodium-ion batteries, Mater. Today Adv. 6 (2020) 100054.
[19] N. Khossossi, R. Ahuja, No-Carbon 2D Anode Materials for Next-Generation Batteries, AIP Publishing LLC AIP Publishing, Melville, New York, 2021.
[20] N. Deng, Y. Feng, G. Wang, X. Wang, L. Wang, Q. Li, L. Zhang, W. Kang, B. Cheng, Y. Liu, Rational structure designs of 2D materials and their applications toward advanced lithium-sulfur battery and lithium-selenium battery, Chem. Eng. J. 401 (2020) 125976.
[21] L. Lin, J. Chen, D. Liu, X. Li, G.G. Wallace, S. Zhang, Engineering 2D materials: A viable pathway for improved electrochemical energy storage, Adv. Energy Mater. 10 (45) (2020) 2002621.
[22] J. Sun, H.-W. Lee, M. Pasta, H. Yuan, G. Zheng, Y. Sun, Y. Li, Y. Cui, A phosphorene–graphene hybrid material as a high-capacity anode for sodium-ion batteries, Nature Nanotechnol. 10 (11) (2015) 980–985.
[23] D. Wei, M.R. Astley, N. Harris, R. White, T. Ryhänen, J. Kivioja, Graphene nanoarchitecture in batteries, Nanoscale 6 (16) (2014) 9536–9540.
[24] Y. Jing, Z. Zhou, C.R. Cabrera, Z. Chen, Graphene, inorganic graphene analogs and their composites for lithium ion batteries, J. Mater. Chem. A 2 (31) (2014) 12104–12122.
[25] Y. Lu, Y. Lu, Z. Niu, J. Chen, Graphene-based nanomaterials for sodium-ion batteries, Adv. Energy Mater. 8 (17) (2018) 1702469.
[26] P. Xiang, X. Chen, W. Zhang, J. Li, B. Xiao, L. Li, K. Deng, Metallic borophene polytypes as lightweight anode materials for non-lithium-ion batteries, Phys. Chem. Chem. Phys. 19 (36) (2017) 24945–24954.
[27] X. Zhang, J. Hu, Y. Cheng, H.Y. Yang, Y. Yao, S.A. Yang, Borophene as an extremely high capacity electrode material for Li-ion and Na-ion batteries, Nanoscale 8 (33) (2016) 15340–15347.
[28] S. Zhao, W. Kang, J. Xue, The potential application of phosphorene as an anode material in Li-ion batteries, J. Mater. Chem. A 2 (44) (2014) 19046–19052.
[29] W. Li, Y. Yang, G. Zhang, Y.-W. Zhang, Ultrafast and directional diffusion of lithium in phosphorene for high-performance lithium-ion battery, Nano Lett. 15 (3) (2015) 1691–1697.
[30] V.V. Kulish, O.I. Malyi, C. Persson, P. Wu, Phosphorene as an anode material for Na-ion batteries: a first-principles study, Phys. Chem. Chem. Phys. 17 (21) (2015) 13921–13928.
[31] S. Mukherjee, G. Singh, Two-dimensional anode materials for non-lithium metal-ion batteries, ACS Appl. Energy Mater. 2 (2) (2019) 932–955.
[32] C. Tang, Y. Min, C. Chen, W. Xu, L. Xu, Potential applications of heterostructures of TMDs with MXenes in sodium-ion and Na–O2 batteries, Nano Lett. 19 (8) (2019) 5577–5586.
[33] D.-X. Song, L. Xie, Y.-F. Zhang, Y. Lu, M. An, W.-G. Ma, X. Zhang, Multilayer ion load and diffusion on TMD/MXene heterostructure anodes for alkali-ion batteries, ACS Appl. Energy Mater. 3 (8) (2020) 7699–7709.
[34] N. Hemanth, T. Kim, B. Kim, A.H. Jadhav, K. Lee, N.K. Chaudhari, Transition metal dichalcogenide-decorated MXenes: promising hybrid electrodes for energy storage and conversion applications, Mater. Chem. Front. 5 (8) (2021) 3298–3321.
[35] K. Watanabe, T. Taniguchi, H. Kanda, Direct-bandgap properties and evidence for ultraviolet lasing of hexagonal boron nitride single crystal, Nature Mater. 3 (6) (2004) 404–409.
[36] H. Şahin, S. Cahangirov, M. Topsakal, E. Bekaroglu, E. Akturk, R.T. Senger, S. Ciraci, Monolayer honeycomb structures of group-IV elements and III-V binary compounds: First-principles calculations, Phys. Rev. B 80 (15) (2009) 155453.
[37] Z. Liu, Y. Gong, W. Zhou, L. Ma, J. Yu, J.C. Idrobo, J. Jung, A.H. MacDonald, R. Vajtai, J. Lou, et al., Ultrathin high-temperature oxidation-resistant coatings of hexagonal boron nitride, Nature Commun. 4 (1) (2013) 1–8.
[38] Y. Kubota, K. Watanabe, O. Tsuda, T. Taniguchi, Deep ultraviolet light-emitting hexagonal boron nitride synthesized at atmospheric pressure, Science 317 (5840) (2007) 932–934.
[39] M. Topsakal, E. Aktürk, S. Ciraci, First-principles study of two-and one-dimensional honeycomb structures of boron nitride, Phys. Rev. B 79 (11) (2009) 115442.
[40] Y. Hwang, Y.-C. Chung, Comparative study of metal atom adsorption on free-standing h-BN and h-BN/Ni (1 1 1) surfaces, Appl. Surf. Sci. 299 (2014) 29–34.
[41] Y. Hwang, Y.-C. Chung, Lithium adsorption on hexagonal boron nitride nanosheet using dispersion-corrected density functional theory calculations, Japan. J. Appl. Phys. 52 (6S) (2013) 06GG08.
[42] S. Demirci, S.E. Rad, S. Kazak, S. Nezir, S. Jahangirov, Monolayer diboron dinitride: Direct band-gap semiconductor with high absorption in the visible range, Phys. Rev. B 101 (12) (2020) 125408.
[43] G. Kresse, J. Furthmüller, Efficient iterative schemes for ab initio total-energy calculations using a plane-wave basis set, Phys. Rev. B 54 (16) (1996) 11169.
[44] J.P. Perdew, K. Burke, M. Ernzerhof, Generalized gradient approximation made simple, Phys. Rev. Lett. 77 (18) (1996) 3865.
[45] J. Heyd, G.E. Scuseria, M. Ernzerhof, Hybrid functionals based on a screened Coulomb potential, J. Chem. Phys. 118 (18) (2003) 8207–8215.
[46] H.J. Monkhorst, J.D. Pack, Special points for Brillouin-zone integrations, Phys. Rev. B 13 (12) (1976) 5188.
[47] G. Henkelman, A. Arnaldsson, H. Jónsson, A fast and robust algorithm for Bader decomposition of charge density, Comput. Mater. Sci. 36 (3) (2006) 354–360.
[48] M. Parrinello, A. Rahman, Crystal structure and pair potentials: A molecular-dynamics study, Phys. Rev. Lett. 45 (14) (1980) 1196.
[49] G. Henkelman, B.P. Uberuaga, H. Jónsson, A climbing image nudged elastic band method for finding saddle points and minimum energy paths, J. Chem. Phys. 113 (22) (2000) 9901–9904.
[50] B. Byles, N. Palapati, A. Subramanian, E. Pomerantseva, The role of electronic and ionic conductivities in the rate performance of tunnel structured manganese oxides in Li-ion batteries, APL Mater. 4 (4) (2016) 046108.
[51] S.-Y. Chung, Y.-M. Chiang, Microscale measurements of the electrical conductivity of doped LiFePO4, Electrochem. Solid State Lett. 6 (12) (2003) A278.
[52] Y.-F. Deng, S.-X. Zhao, Y.-H. Xu, K. Gao, C.-W. Nan, Impact of P-doped in spinel LiNi0. 5Mn1. 5O4 on degree of disorder, grain morphology, and electrochemical performance, Chem. Mater. 27 (22) (2015) 7734–7742.

[53] C.R. Dean, A.F. Young, I. Meric, C. Lee, L. Wang, S. Sorgenfrei, K. Watanabe, T. Taniguchi, P. Kim, K.L. Shepard, et al., Boron nitride substrates for high-quality graphene electronics, Nature Nanotechnol. 5 (10) (2010) 722–726.
[54] N. Khossossi, Y. Benhouria, S.R. Naqvi, P.K. Panda, I. Essaoudi, A. Ainane, R. Ahuja, Hydrogen storage characteristics of Li and Na decorated 2D boron phosphide, Sustain. Energy Fuels 4 (9) (2020) 4538–4546.
[55] H. Jiang, W. Shyy, M. Liu, L. Wei, M. Wu, T. Zhao, Boron phosphide monolayer as a potential anode material for alkali metal-based batteries, J. Mater. Chem. A 5 (2) (2017) 672–679.
[56] S. Wang, W. Zhang, C. Lu, Y. Ding, J. Yin, P. Zhang, Y. Jiang, Enhanced ion diffusion induced by structural transition of Li-modified borophosphene, Phys. Chem. Chem. Phys. 22 (37) (2020) 21326–21333.
[57] N. Khossossi, A. Banerjee, Y. Benhouria, I. Essaoudi, A. Ainane, R. Ahuja, Ab initio study of a 2D h-BAs monolayer: a promising anode material for alkali-metal ion batteries, Phys. Chem. Chem. Phys. 21 (33) (2019) 18328–18337.
[58] X. Zhang, L. Jin, X. Dai, G. Chen, G. Liu, Two-dimensional GaN: An excellent electrode material providing fast Ion diffusion and high storage capacity for Li-ion and na-ion batteries, ACS Appl. Mater. Interfaces 10 (45) (2018) 38978–38984.
[59] D. Er, J. Li, M. Naguib, Y. Gogotsi, V.B. Shenoy, Ti3C2 MXene as a high capacity electrode material for metal (Li, Na, K, Ca) ion batteries, ACS Appl. Mater. Interfaces 6 (14) (2014) 11173–11179.
[60] Q. Tang, Z. Zhou, P. Shen, Are MXenes promising anode materials for Li ion batteries? Computational studies on electronic properties and Li storage capability of Ti3C2 and Ti3C2X2 (X=F, OH) monolayer, J. Am. Chem. Soc. 134 (40) (2012) 16909–16916.
[61] Y. Li, D. Wu, Z. Zhou, C.R. Cabrera, Z. Chen, Enhanced Li adsorption and diffusion on MoS2 zigzag nanoribbons by edge effects: a computational study, J. Phys. Chem. Lett. 3 (16) (2012) 2221–2227.
[62] N. Khossossi, V. Shukla, Y. Benhouria, I. Essaoudi, A. Ainane, R. Ahuja, G. Babu, P.M. Ajayan, Exploring the possibility of β-phase arsenic-phosphorus polymorph monolayer as anode materials for sodium-ion batteries, Adv. Theory Simul. 3 (8) (2020) 2000023.
[63] X. Zhang, Z. Yu, S.-S. Wang, S. Guan, H.Y. Yang, Y. Yao, S.A. Yang, Theoretical prediction of MoN 2 monolayer as a high capacity electrode material for metal ion batteries, J. Mater. Chem. A 4 (39) (2016) 15224–15231.
[64] H. Lin, G. Liu, L. Zhu, Z. Zhang, R. Jin, Y. Huang, S. Gao, Flexible borophosphene monolayer: A potential Dirac anode for high-performance non-lithium ion batteries, Appl. Surf. Sci. 544 (2021) 148895.
[65] Y. Zhang, E.-H. Zhang, M.-G. Xia, S.-L. Zhang, Borophosphene as a promising Dirac anode with large capacity and high-rate capability for sodium-ion batteries, Phys. Chem. Chem. Phys. 22 (36) (2020) 20851–20857.
[66] Y. Wang, Y. Li, Ab initio prediction of two-dimensional Si 3 C enabling high specific capacity as an anode material for Li/Na/K-ion batteries, J. Mater. Chem. A 8 (8) (2020) 4274–4282.
[67] X. Zhang, L. Jin, X. Dai, G. Chen, G. Liu, A record-high ion storage capacity of T-graphene as two-dimensional anode material for Li-ion and Na-ion batteries, Appl. Surf. Sci. 527 (2020) 146849.
[68] K. Toyoura, Y. Koyama, A. Kuwabara, F. Oba, I. Tanaka, First-principles approach to chemical diffusion of lithium atoms in a graphite intercalation compound, Phys. Rev. B 78 (21) (2008) 214303.
[69] R. Yazami, Y.F. Reynier, Mechanism of self-discharge in graphite–lithium anode, Electrochim. Acta 47 (8) (2002) 1217–1223.
[70] J. Hu, B. Xu, C. Ouyang, Y. Zhang, S.A. Yang, Investigations on Nb 2 C monolayer as promising anode material for Li or non-Li ion batteries from first-principles calculations, RSC Adv. 6 (33) (2016) 27467–27474.
[71] X. Deng, X. Chen, Y. Huang, B. Xiao, H. Du, Ab initio characterization of layered MoS2 as anode for sodium-ion batteries, J. Phys. Chem. C 123 (2019) 4721–4728.
[72] S. Mukherjee, L. Kavalsky, C.V. Singh, Ultrahigh storage and fast diffusion of Na and K in blue phosphorene anodes, ACS Appl. Mater. Interfaces 10 (10) (2018) 8630–8639.
[73] Q. Zhang, J. Ma, M. Lei, R. Quhe, Metallic MoN layer and its application as anode for lithium-ion batteries, Nanotechnology 29 (16) (2018) 165402.
[74] V. Wang, N. Xu, J.C. Liu, G. Tang, W.-T. Geng, VASPKIT: a user-friendly interface facilitating high-throughput computing and analysis using VASP code, 2019, arXiv preprint arXiv:1908.08269.
[75] T.V. Vu, A. Kartamyshev, N.V. Hieu, T.D. Dang, S.-N. Nguyen, N. Poklonski, C.V. Nguyen, H.V. Phuc, N.N. Hieu, Structural, elastic, and electronic properties of chemically functionalized boron phosphide monolayer, RSC Adv. 11 (15) (2021) 8552–8558.
[76] G.-C. Guo, R.-Z. Wang, B.-M. Ming, C. Wang, S.-W. Luo, M. Zhang, H. Yan, C 3 N/phosphorene heterostructure: a promising anode material in lithium-ion batteries, J. Mater. Chem. A 7 (5) (2019) 2106–2113.
[77] Y. Li, W. Wu, F. Ma, Blue phosphorene/graphene heterostructure as a promising anode for lithium-ion batteries: a first-principles study with vibrational analysis techniques, J. Mater. Chem. A 7 (2) (2019) 611–620.
[78] H. Şahin, S. Cahangirov, M. Topsakal, E. Bekaroglu, E. Akturk, R.T. Senger, S. Ciraci, Monolayer honeycomb structures of group-IV elements and III-V binary compounds: First-principles calculations, Phys. Rev. B 80 (15) (2009) 155453.